Directed yeast genome evolution by controlled introduction of trans-chromosomic structural variations

Bin Jia[1,2,*] , Jin Jin[1, 2,*] , Ming-Zhe Han[1, 2], Bing-Zhi Li[1, 2] & Ying-Jin Yuan[1,2,†]

[1] Frontier Science Center for Synthetic Biology and Key Laboratory of Systems Bioengineering (Ministry of Education), School of Chemical Engineering and Technology, Tianjin University, 300072 Tianjin, China.

[2] Collaborative Innovation Center of Chemical Science and Engineering (Tianjin), Tianjin University, 300072 Tianjin, China.

[*] Authors contributed equally to this work.

[†] Corresponding author (email: yjyuan@tju.edu.cn)

ABSTRACT

Naturally occurring structural variations (SVs) are a considerable source of genomic variation and can reshape chromosomes 3D architecture. The synthetic chromosome rearrangement and modification by loxP-mediated evolution (SCRaMbLE) system has been proved to generate random SVs to impact phenotypes and thus constitutes powerful drivers of directed genome evolution. However, how to reveal the molecular mechanism insights into the interactions between phenotypes and complex SVs, especially inversions and translocations, has so far remained challenging. In this study, we develop a SV-prone yeast strain by using SCRaMbLE with two synthetic chromosomes, synV and synX. An heterologous biosynthesis pathway allowing a high

throughput screen for increased yield of astaxanthin is used as readout and a proof of concept for the application of SV in industry. We report here that complex SVs, including a pericentric inversion and a trans-chromosomes translocation between synV and synX, result in two neochromosomes and a 2.7-fold yield of astaxanthin. We demonstrated that inversion and inversion reshaped chromosomes 3D architecture and led to large reorganization of the genetic information nearby the breakpoint of the SVs along the chromosomes. Specifically, the pericentric inversion increased the expression of STE18 and the trans-chromosomic translocation increased the expression of RPS5 and MCM22, which contributed to higher astaxanthin yield. We also used the model learned from the aforementioned random screen and successfully harnessed the precise introduction of trans-chromosomes translocation and pericentric inversions by rational design. Overall, our work provides an effective tool to not only accelerate the directed genome evolution but also reveal mechanistic insight of complex SVs for altering phenotypes.

Key words: Directed genome evolution, Structural variations, SCRaMbLE, Pericentric inversion, Trans-chromosomes translocation

Introduction

Chromosomes are highly dynamic objects that often undergo large structural variations(SVs), which in turn can reshape chromosomes and impact phenotypes(Pevzner and Tesler 2003; Dujon et al. 2004; Redon et al. 2006; Darling et

al. 2008; Kidd et al. 2008; Conrad et al. 2010; Dujon 2010; Pang et al. 2010; Henssen et al. 2017; Yue et al. 2017; Peter et al. 2018). Naturally occurring SVs comprised both unbalanced SVs that are copy number variations including deletions and duplications, and balanced SVs that are copy number neutral including inversions and translocations(Fleiss et al. 2019). Both the unbalanced SVs and balanced SVs can modify the 3D architecture of the chromosomes and potentially affect genetic functioning, which contributed to the genome evolution. For example, Selmecki.et al showed tetraploids yeast undergo significantly faster adaptation in a poor carbon source environment with larger deletion of chromosomes. (Selmecki et al. 2015). Li.et al found that deletion of left arm of synthetic chromosome X and duplication of chromosome VIII (trisomy) lead to increased rapamycin resistance in yeast(Li et al. 2019). With the development of genome medicine, it is indicated reciprocal translocation between chromosomes have contributed to several human diseases, for instance, chronic myeloid leukemia (chromosomes 9 with 22) and Mobius-like syndrome (chromosomes 1 with 2)(Eyupoglu et al. 2016) (Nishikawa et al. 1997). In addition, pericentric inversion of chromosome 9 is one of the most common chromosomal abnormalities and can be associated with ambiguous genitalia in children(Sotoudeh et al. 2017). It is challenge to map the balanced SVs than unbalanced SVs due to the copy number neutral. So far, the detailed molecular mechanism underlying balanced SVs remained unexplored due to lack of cell models.

The baker yeast (Saccharomyces cere*visiae*) appreciated for the availability of its powerful genetic tools, biosafety and fast growth rate has been used extensively in

67 synthetic biology for industrial purposes. High-throughput phenotypic screenings have
68 been employed to identify genome-wide deletions and duplications that increase the
69 yield of yeast synthetic biology products. The completion of the yeast gene-knockout
70 collection (YKOC) has enabled the analysis of synthetic genetic interactions(Puddu et
71 al. 2019). The construction of segmental duplications covering the whole *S. cerevisiae*
72 genome has been used to produce strains with enhanced tolerance to
73 stresses(Natesuntorn et al. 2015). Many rational design strategies, including
74 overexpression and downregulation, are time-consuming because identifying gene
75 targets remains an challenge due to the complexity of genetic networks (Si et al.
76 2015)[Rapid prototyping of microbial cell factories via genome-scale engineering.
77 Biotechnol Adv 2015, 33:1420-1432.]. Many successful examples demonstrate that the
78 synthetic yeast chromosome could be reprogrammed for various purposes with greatly
79 enhanced metabolic capacity(Jia et al. 2018; Shen et al. 2018; Wu et al. 2018). The
80 Synthetic Chromosome Rearrangement and Modification by LoxP-mediated Evolution
81 (SCRaMbLE) technology have been developed to generate larger-scale SVs(Blount et
82 al. 2018; Jia et al. 2018; Liu et al. 2018; Luo et al. 2018; Shen et al. 2018; Wang et al.
83 2018; Wu et al. 2018; Li et al. 2019; Ma et al. 2019; Gowers et al. 2020). SCRaMbLE
84 is a powerful approach to study how chromosomal architecture impacts phenotypes and
85 can be to mimic the Darwinian evolution process in the test tube for targeted phenotypes.
86 Thus, SCRaMbLE can be viewed as natural molecular tools for directed genome
87 evolution by iterative rounds of mutagenesis and screening or selection on the genome
88 scale. So far, SCaMbLE has been used for directed genome evolution mainly with

signal synthetic chromosome.

In this work we report that one by using SCaMbLE and two synthetic chromosomes, can for the first time creates chromosome inversion and translocation events on a larger scale and at a higher frequency. Introducing the same yeast cell with two synthetic chromosomes, each containing hundreds of non-directional loxPsym sites positioned downstream of non-essential genes and major landmarks provides a novel approach to genome reorganization especially SVs. We evaluate the effects of SVs on the enhanced production of an exogenous but commercially valuable terpenoid, astaxanthin. Two cycles of SCRaMbLE were used to iteratively generate complex SVs and improve the astaxanthin yield. We used the high-resolution chromosome conformational capture (Hi-C) sequencing approach to investigate the 3D conformations of chromosomes with complex SVs(Akdemir et al. 2020), and observed an inversion spanning the centromere and a translocation between synV and synX. We developed a method to precisely reconstitute the translocations and inversions, and recaptured their combined effects on increasing the yield of astaxanthin by 2.7-fold. Our work thus provides a new toolkit for directed evolution of genomic assembly and reorganization.

Results

SCRaMbLE with two synthetic chromosomes for directed genome evolution

To investigate more complex SVs and biosynthesis pathways, we used the haploid strain SYN510 containing both synV with 176 loxPsym sites(Xie et al. 2017) and synX with 245 loxPsym sites(Wu et al. 2017c) for the biosynthesis of astaxanthin.

111 Astaxanthin is the end metabolite of the MVA pathway; it has tremendous antioxidant
112 activity and is widely used in nutraceuticals, cosmetics and aquaculture(Ambati et al.
113 2014; Igielska-Kalwat et al. 2015). The astaxanthin biosynthesis pathway consists of 5
114 genes. *CrtE*, *CrtI* and *CrtYB* are involved in carotenoid biosynthesis, after which a
115 reticular metabolic pathway with β-carotene ketolase (CrtW) and β-carotene
116 hydroxylase (CrtZ) performs a two-step hydroxylation and ketolation
117 reaction(Supplementary information, Fig. 1a). Our previous study demonstrated that
118 the combination of Aa_CrtZ–BDC263_CrtW showed lower intermediate accumulation
119 and achieved better astaxanthin yield(Wang et al. 2017). To increase the stability of the
120 astaxanthin biosynthesis pathway, all five genes were assembled together and integrated
121 at the *YEL063C*/*CAN1* locus of synV to generate the yeast strain YJJ001 (Fig. 1a). It
122 has been reported that the pCRE4 plasmid (pGal1-Cre-EBD-tCYC1) has tight control
123 of Cre recombinase and can be used for Multiplex SCRaMbLE Iterative Cycling
124 (MuSIC). Thus, the pCRE4 plasmid with a Ura3 marker was transformed into YJJ001
125 for the control of SCRaMbLE.
126
127 In the first cycle of SCRaMbLE, strain YJJ168 was selected from the SCRaMbLEd
128 yeast pool due to its dark red pigmentation (Supplementary information, Fig. 1b). To
129 generate more complicated SVs and the desired phenotype, we used YJJ168 for the
130 second cycle of SCRaMbLE to yield another SCRaMbLEd strain, YJJ432. To identify
131 the chromosome SVs in haploids caused by SCRaMbLE, we deep sequenced YJJ168
132 and YJJ432. As shown in Fig. 1a and Supplementary information, Fig. 2, a 3 kb deletion

133 (YJL218W-YJL217W), a 1 kb inversion (YER044C) and a 210 kb pericentric inversion
134 (YJL052C-A-YJR071C) with 127 genes were observed in the SCRaMbLEd strain
135 YJJ168. It is interesting that the upstream and downstream of inversions of YJL052C-
136 A-YJR071C were on the left arm and right arm of synX, respectively. In other words,
137 this inversion spanned the centromere of synX. As an iterated SCRaMbLEd strain from
138 YJJ168, YJJ432 was observed to contain not only all the same SVs as YJJ168 but also
139 a inversion of YJL170C-YJL158C and a trans-chromosomictranslocation. It is noted
140 that the trans-chromosomictranslocation caused an exchange of 59 kb from the right
141 arm of synV and 74 kb from the right arm of synX that had not previously been reported.
142 From the sequencing data above, we find that the second-generation strains can inherit
143 genotypic SVs from first-cycle SCRaMbLEd strains. PCR verification of novel
144 junctions also confirmed that inversion and translocation events occurred in YJJ168 and
145 YJJ432 (Supplementary information, Fig. 3).
146
147 To investigate the structural organization of the chromosome SVs, Hi-C contact maps
148 (Fig. 1b) and 3D representations (Fig. 1c) of synV and synX were generated from
149 YJJ001, YJJ168 and YJJ432. The contact maps of synV and synX in YJJ168 and
150 YJJ432 showed several new interactions, indicating large-scale rearrangements in both
151 SCRaMbLEd strains. YJJ168 exhibited a new interaction indicating a large inversion
152 (YJL052C-A-YJR071C) event. The contact map of YJJ432 revealed three new
153 interactions caused by the large inversion (YJL052C-A-YJR071C), one inversion
154 (YJL170C-YJL158C) in synX and one translocation between the right arm of synV

155 (YJR130C) and the right arm of synX (YER164W). A three-dimensional model of the
156 16 yeast chromosomes and amplified chromosomes of synV and synX are provided in
157 Fig. 1c. The centromeres gather at the spindle pole, and all chromosomes are clustered
158 by the centromeres at one pole of the nucleus. The telomeres are clustered at the other
159 end. The 3D representations show that the average trajectories of chromosomes in
160 YJJ168 and YJJ432 did not appear to be substantively altered compared with those in
161 YJJ001, with the synthetic chromosomes neighboring the same chromosomes as the
162 native ones. New connections were generated in synX of strain YJJ168 and strain
163 YJJ432 due to the inversion spanning the centromere. In strain YJJ432, the right arms
164 of synV and synX generate two new connections because of the translocation between
165 synV and synX (the area within the dashed oval). It is indicated that the translocation
166 on the right arm of synV has a closer spatial distance with synX and consequently has
167 stronger interactions.
168
169 Meanwhile, the two SCRaMbLEd strains and YJJ001 were subjected to fermentation
170 experiments in YPD medium, and the astaxanthin yield was analyzed by high-
171 performance liquid chromatography (HPLC). As illustrated in Fig. 1d, the astaxanthin
172 yield in strain YJJ001 was 0.61 mg/g DCW, and the astaxanthin yield of the two
173 SCRaMbLEd strains (YJJ168 and YJJ432) was increased, to 0.90 and 2.7 mg/g DCW,
174 respectively. The astaxanthin yield was increased 1.48- to 4.43-fold in the SCRaMbLEd
175 strains compared with the nonSCRaMbLEd parent strain. These results revealed the
176 new interactions of synthetic chromosomes in SCRaMbLEd strains via Hi-C

technology. SCRaMbLE strains provide sufficiently detectable SVs, indicating that the SCRaMbLE system provides a driving force to alter cell phenotypes through rearranging gene order and number.

Reorganization of the genetic information on the regions of SVs

The pericentric inversion and trans-chromosomic translocation alter the spatial positions of the breakpoint-flanking regions, which may which may led to large reorganization of the genetic information along the chromosomes. To explore whether the genetic information in the breakpoint-flanking regions were affected, we examined transcription profile on the 20 kb regions upstream and downstream of the two loxPsym breakpoints. As shown in Fig. 2a, the upstream and downstream regions of the breakpoints of the pericentric inversion in YJJ168 were named A, B, C, and D, respectively. We first observed changes in the transcription levels of YJL053W, YJL052C-A and YJL052W near the left breakpoint and the transcription levels of YJL067C, YJL070C and YJL071W near the right breakpoint. In the whole 80 kb region consisting of A, B, C and D, 19 of 51 genes showed changes in expression compared with the control strain YJJ001(Log2FoldChange > 1-fold), with 1 gene of YJL052W downregulated and 18 genes (YJL053W, YJL052C-A, YJL049W, YJL046W, YJL045W, YJR067C, YJR068W, YJR070C, YJR071W, YJR072C, YJR076C, YJR079W, YJR080C, YJR082C, YJR085C, YJR086C, YJR087W and YJR088C) upregulated, respectively. Around the left breakpoint, the changes in YJL052C-A and YJL052W were the most obvious, whereas around the right arm recombination site, the

199 change in YJR070C was the most obvious. Similarly, the regions upstream and
200 downstream of the breakpoint in the right arm of synV and the breakpoint in the right
201 arm of synX in YJJ432 were labeled E, F, G, and H, respectively (Fig. 2b). Compared
202 with the control strain, 14 of the 38 genes in these regions exhibited changed
203 expression(Log2FoldChange > 1-fold), with 2 genes (YER158C and YJR127C)
204 downregulated and 12 genes (YER156C, YER163C, YER168C, YER170W, YJR122W,
205 YJR123W, YJR125C, YJR129C, YJR133W, YJR135C, YJR135W-A, YJR136C)
206 upregulated, respectively. The results indicated that the expression of genes in the
207 breakpoint-flanking regions was indeed affected by different types of SVs. To further
208 quantify the interactions of the recombination sites, we counted the interaction values
209 of the four points on the interaction matrix of YJJ168 and YJJ432 and counted the
210 differences between different interaction domains (areas marked by boxes in
211 Supplementary information, Fig. 4). As the results show, regions A and C and regions
212 B and D had significant interactions in inversion strains YJJ168 and YJJ432. In
213 translocation strain YJJ432, the interactions of regions E and H and F and G were
214 increased as a result of the greater proximity of the right arm of synV (YJR130C) to
215 synX and the right arm of synX (YER164W) to synV. These results further indicate that
216 two sites that are closer in space have greater interaction. It is spectacular that the
217 pericentric inversions and trans-chromosomes translocation changed larger number of
218 genes position and the transcription direction, which affected the transcription levels of
219 genes in the regions nearby the breakpoint of SVs(Wu et al. 2017b).

220 **Mapping of genetic targets contributing to higher astaxanthin yield**

To identify the genetic targets with regard to the improvement of astaxanthin yield, the above down-regulated genes and up-regulated genes in the regions nearby the breakpoint of SVs were knocked out and overexpressed in the strain YJJ001 for fermentation assay, respectively(Table 1). As illustrated in Fig. 3a, compared to the control strain, astaxanthin yields were significantly increased in strains with YJR086W, YJR123W and YJR135C over-expression strain. The function of these three genes are briefly described in Table 2. Although the exact reason for these genes to be beneficial to astaxanthin yield remains to be elucidated, it is possible to speculate the mechanism resulting in the favorable changes of this phenotype from functions previously described in the literature. The result indicated upregulated these genes have contributed to higher astaxanthin yield.

To further explore the global affection of chromosomal rearrangements on metabolic pathways, enrichment analysis of transcriptomics was used to identify differentially transcribed genes with known functions involved in KEGG pathways. Several genes involved in terpenoid backbone biosynthesis, ergosterol biosynthesis and citrate cycle were upregulated in the YJJ168 and YJJ432 (Fig. 3b). In SCRaMbLEd strain YJJ168, the upregulated genes ERG24, ERG25, ERG26 and ERG27 were involved in ergosterol biosynthesis, while ERG10, ERG20 and BTS1 were involved in terpenoid backbone biosynthesis. In YJJ432, ERG24, ERG26 and ERG27, which are involved in the biosynthesis of ergosterol, and ERG10, ERG12, ERG20 and BTS1, which are involved in terpenoid backbone biosynthesis, were found to be upregulated. As a consequence, these two pathways could increase the flux of the MVA pathway and cell storage

243 capacity of hydrophobic carotenoids(Gao et al. 2017; Wu et al. 2017a). The
244 improvement of citrate cycle could provide sufficient reducing power and energy for
245 the MVA pathway. These transcriptome analyses indicated that the improved yield of
246 astaxanthin was caused by the upregulation of these genes, further clarifying the direct
247 effect of the SVs on astaxanthin accumulation. The results demonstrated the SVs can
248 led to large reorganization of the genetic information along the chromosomes and
249 accelerate the directed genome evolution with selection of targeted phenotypes.
250

251 **Rational introduction of inversion and translocation in yeast**

252 To verify the effect of the pericentric inversion and trans-chromosomic translocation,
253 we developed a method to rationally generate these inversions and translocations. First,
254 we constructed an astaxanthin-producing strain named YJJ468 from the wild-type
255 strain BY4741 by integrating the biosynthesis pathway of astaxanthin at the
256 *YEL063C*/*CAN1* locus of chromosome V. Then, we designed an on/off switch
257 consisting of two markers (URA3 and Hyg). As shown in Fig. 4a, the URA3 promoter
258 was inserted upstream of loxP site 1, and the open reading frame of URA3 was inserted
259 downstream of loxP site 1, allowing the expression of URA3. Hyg without a promoter
260 was positioned immediately downstream of loxP site 2. A complete HIS3 marker was
261 positioned upstream of loxP site 2 as a selection marker to help loxP-Hyg integrate into
262 the chromosome. The pGal1-Cre-EBD-tCYC1 plasmid with a G418 marker was
263 transformed into strain YJJ468 (Supplementary Fig. 7). The activation of Cre
264 recombinase will catalyze the recombination of the two loxP sites, leading to a change

265 in the phenotype of the yeast from Hyg- to Hyg+. Consequently, hygromycin media
266 could be used to select translocation and inversion strains. Using the above approach,
267 strain YJJ473 with pericentric inversion and strain YJJ474 with trans-chromosomic
268 translocation were generated and isolated by screening on SC-hygromycin agar plates.
269 Strains YJJ473 and YJJ474 were further analyzed using whole-genome sequencing to
270 verify the genomic variations produced by the recombination. As Fig. 4a shows, the
271 inversion and translocation region had breakpoints at the loxP sites in YJJ473 and
272 YJJ474, indicating that the desired inversion and translocation were artificially
273 recreated from the wild-type strain YJJ468.
274 Meanwhile, PCR was used to further verify the inversion and translocation. Before
275 recombination, sequences in YJJ468 could be amplified by primer pairs 1/2, 3/4, 5/6,
276 and 7/8. After recombination, sequences in YJJ473 could be amplified by primer pairs
277 1/3 and 2/4, while sequences in YJJ474 could be amplified by primer pairs 5/8 and 6/7
278 (Fig. 4b). Therefore, we can confirm that inversion and translocation events occurred
279 in YJJ473 and YJJ474. Compared to the initial strain yJJ468, YJJ473 and YJJ474 had
280 enhanced astaxanthin production phenotypes, yielding 1.11 mg/g DCW and 1.28 mg/g
281 DCW, respectively, which were similar to those of the SCRaMbLEd strains (Fig. 4c).
282 YJJ473 and YJJ474 increased the astaxanthin yield 1.8- and 2.1-fold relative to the
283 parent strain YJJ468. These results indicated that the YJL052C-A-YJR071C inversion
284 and YJR130C-YER164W translocation increased the production of astaxanthin and
285 were responsible for the enhanced astaxanthin production phenotypes of SCRaMbLE
286 strains yJJ168 and yJJ432. The results indicated that the YJL052C-A-YJR071C

287 inversion and YJR130C-YER164W translocation contributed to the improvement of
288 astaxanthin production. It is anticipated that we can used the model learned from the
289 random screen of SCRaMbLE and successfully harnessed the precise introduction of
290 pericentric inversions and trans-chromosomic translocation by rational design.
291

292 **Discussion**

293 Our study focused on investigating complex chromosome SVs by enabling haploid
294 yeast containing multiple synthetic chromosomes to be SCRaMbLEd, which has
295 significant advantages over pre-existing methods for laboratory evolution. First,
296 traditional evolution approaches, such as physical mutagenesis or chemical
297 mutagenesis, typically cause hundreds of single nucleotide polymorphisms (SNPs) or
298 insertions and deletions (indels)(Jin et al. 2018), which make it difficult to confirm the
299 targets responsible for observed changes in phenotypes. In comparison, SCRaMbLE
300 has been demonstrated to rapidly generate larger scale SVs, providing clear targets to
301 verify and understand more deeply. In this study, we have demonstrated that pathway-
302 doubling is not the only way to increase yield (Jia et al. 2018), changes in map position
303 and direction of endogenous genes can also affect yield. Second, the synthetic yeast
304 project (Sc2.0) aims to synthesize 16 yeast chromosomes, each of which contains
305 hundreds of loxPsym sites, downstream of every nonessential gene. Our research has
306 shown that SCRaMbLE with two synthetic chromosomes can generate translocations
307 between two synthetic chromosomes. Thus, it is anticipated that the integration of
308 multiple synthetic chromosomes will extend the diversity and quantity of SVs.

309 Moreover, SCRaMbLE with multiple synthetic chromosomes provided a powerful
310 model in which to investigate the trajectory of chromosome SVs during iterative
311 evolution. In this study, YJJ432 not only inherited the inversion spanning the
312 centromere from YJJ168 but also acquired new genetic changes, namely, a translocation
313 between two synthetic chromosomes.
314
315 The SCRaMbLE system provided sufficiently large structural variations to allow us to
316 analyze novel interactions and structures via Hi-C technology. The translocation strain
317 YJJ474 on the right arm of synV (YJR130C) has a closer spatial distance with synX
318 and consequently has stronger interactions. Chromosomal SVs cause changes in the 3D
319 architecture of the genome and potentially alter cellular functions. The development of
320 the 3C technique and its derivatives has provided a toolbox that enables the systematic
321 spatial interrogation of multiple loci or even the entire genome(Lieberman-Aiden et al.
322 2009; Dekker et al. 2013). Based on genome-wide high-throughput chromosome
323 conformation capture (Hi-C) technology, a 2D heat map can be constructed to indicate
324 the frequency of interaction between two points in the genome. Depending on their
325 positions, SVs often change the Hi-C profile of a locus, leaving specific signatures that
326 can be analyzed further(Burton et al. 2013; Bianco et al. 2018). For example, deletions
327 can result in novel interactions between two regions that were previously separated,
328 whereas inversions result in a characteristic ‘bow tie’ configuration when mapped onto
329 a reference genome. Furthermore, owing to its proximity-ligation nature, the Hi-C is
330 also suitable for the identification of SVs without a priori knowledge(Rickman et al.

331 2012; Burton et al. 2013; Rao et al. 2014; Harewood et al. 2017).

332

333 SCRaMbLEing two synthetic chromosomes generated random and complex SVs,
334 which reshaped chromosomes 3D architecture. Duan.et al reported that the genome 3D
335 structure affected genes expressions(Duan et al. 2010) It is known that telomeres and
336 centromeres could inhibit the expression of genes nearby (Chen and Zhang 2016), while
337 the autonomously replicating sequence (ARS) could increase the expression of genes
338 nearby(Flagfeldt et al. 2009). In the study, the pericentric inversions and trans-
339 chromosomes translocation changed the map position of centromeres in chromosome
340 X and caused the exchange of the right telomeres of chromosome V with chromosome
341 X, respectively. Thus, larger number of genes position and the transcription direction,
342 which affected the transcription levels of genes in the regions nearby the breakpoint of
343 SVs. It is demonstrated that over-expression of YJR086W(STE18), YJR123W(RPS5)
344 and YJR135C(MCM22) improved astaxanthin yield. Choudhury.et al show that
345 phosphorylation of the yeast Gg subunit (Ste18) can serve as intrinsic regulators of G
346 protein signaling and differentially activates mitogen-activated protein kinases
347 (MAPKs) pathway (Choudhury et al. 2018), which potentially mediates the activation
348 of some transcription factors and metabolic network related to the astaxanthin
349 biosynthesis. Ghosh.et al reported Rps5 is an essential gene coding a protein component
350 of the small (40S) ribosomal subunit. Over-expression of Rps5 potentially impact the
351 translation initiation of yeast S. cerevisiae (Saliba et al. 2014), which may increase the
352 translation of some genes being beneficial to the astaxanthin biosynthesis. Poddar.et al

353 demonstrated MCM22 involved in chromosome segregation, mutations of which
354 caused a decrease in the stability of the minichromosome . Over-expression of MCM22
355 potentially maintained the stability of chromosome during segregation and enhanced
356 the cell viability during fermentation(Poddar et al. 1999). The exact mechanism of over-
357 expression of STE18, RPS5 and MCM22 contributing to astaxanthin biosynthesis is
358 unknown, however, upregulation of these genes may be beneficial for tuning metabolic
359 network, the translation initiation process and stability of chromosome during
360 segregation, which may explain why this genes affects astaxanthin biosynthesis.
361
362 In this manuscript, we have developed both a random method and a rational method to
363 generate complex SVs. The random method uses SCRaMbLE in yeast with two
364 synthetic chromosomes to generate yeast libraries containing complex SVs for
365 screening desired phenotypes. The rational method enables a selection marker to switch
366 from transcriptionally “off” to transcriptionally “on”. The rational method provides a
367 convenient way to determine the effects of translocation and inversion targets on strain
368 phenotypes. In addition, inversion and translocation strains generated from wild-type
369 strains can be used as materials to study open genetic questions, such as whether
370 inversion and translocation strains become reproductively isolated from control strains.
371 By this method, we validated a larger fragment translocation (right arm of synV
372 (YJR130C) and right arm of synX (YER164W)) and an inversion (YJL052C-A-
373 YJR071C) in wild-type strains and found that both the translocation and inversion
374 increased the yield of astaxanthin. This strategy is potentially a powerful tool for

inducing the recombination of any two positions on chromosomes. How nature evolves with great biodiversity and nurtures organisms containing various numbers of chromosomes is not known. Our work may spark interest and provide a new handle for researchers to study this fundamental biological problem.

382 ## Methods

383 **Strains and media.**

384 All yeast strains used in this study are described in Table 1. The strain SYNVX carries
385 a synV, and a synX is derived from BY4741 (*MATa leu2Δ0 met15Δ0 ura3Δ0 his3Δ1*).
386 BY4741 was used as the initial strain to reconstruct the translocations and inversions
387 caused by SCRaMbLE of the strains and verify targets of astaxanthin yield
388 improvement.

389 Yeast strains were cultured in YPD medium (10 g l^{-1} yeast extract, 20 g l^{-1} peptone,
390 and 20 g l^{-1} glucose). SGal-Ura (synthetic media lacking uracil with 20 g l^{-1} galactose)
391 with 1 μM β-estradiol was used to induce SCRaMbLE. SC medium containing 1 g L−1
392 5-FOA was used to screen strains without the URA3 marker. All yeast solid media
393 contained 20 g L−1 agar. β-Estradiol and 5-FOA were purchased from Sigma-Aldrich.
394 *E. coli* DH5α purchased from BEIJING Biomed Co., Ltd. was used for plasmid
395 construction and replication. *E. coli* were cultivated at 37 °C in Luria–Bertani (LB)
396 complete medium. Kanamycin (50 μg/mL) or ampicillin (100 μg/mL) was added to the
397 medium for selection.

398

399 **Construction of plasmids and strains.**

400 YJJ001 (astaxanthin-producing control strain) was constructed by homologous
401 recombination in SYNVX, directed by 500-bp CAN1 and 500-bp delta site genomic
402 sequences flanking crtE-crtI-crtYB-crtZ-crtW-LEU2. YJJ002 was constructed by
403 transforming YJJ001 with pCRE4 (Supplementary Fig. 1, Supplementary Data 2),

404 followed by selection on SC-URA agar. Overexpression plasmids were constructed by
405 Gibson assemble. The gene knockout cassette (left homologous arm-URA3-right
406 homologous arm) was assembled by overlap extension PCR (OE-
407 PCR).Transformations were performed using the standard lithium acetate
408 procedure(Gietz et al. 1995).
409
410 **SCRaMbLE.**
411 YJJ002 containing the inducible Cre plasmid pGal1-Cre-EBD-tCYC1 was grown
412 overnight in 5 mL SC-Ura media (30 °C, 250 r.p.m. shaking). Then, the cells were
413 harvested and washed three times with sterile water to wash out glucose, and the culture
414 was diluted to an OD600 of 0.6-1.0 in 3 mL SGal-Ura medium. Then, 1 μmol L^{-1} β-
415 estradiol was added to the cultures to induce SCRaMbLE for 6 h (30 °C, 250 r.p.m.
416 shaking). Cells were washed twice by centrifugation, resuspended in sterile water,
417 diluted 5,000-fold, and plated on SC-Ura. The plates were incubated at 30 °C for 60 h.
418
419 **HPLC analysis of astaxanthin production.**
420 SCRaMbLE strains with darker colors were selected for fermentation in shake flasks.
421 Three independent colonies of each strain were inoculated into 5 ml of YPD medium
422 and grown at 30 °C until the OD 600≈ 8.0 (approximately 24 h). Then, the seed culture
423 was transferred into 50 mL fresh YPD with 40 g l^{-1} glucose medium at an initial OD
424 600 of 0.1 and grown until ready to harvest.
425 Astaxanthin was extracted from HCl–heat treated cells with acetone according to Zhou

426 et al. (Zhou et al. 2015) and Wang et al. (Wang et al. 2017) . Carotenoids were extracted
427 as described below. Cells from 2 mL culture were collected and washed with distilled
428 water. Then, the cells were resuspended in 1 mL of 3 M HCl, boiled for 5 min, and
429 subsequently cooled in an ice bath for 5 min. After that, the cell debris was washed
430 twice with distilled water and resuspended in 0.5 mL of acetone containing 1% (wv^{-1})
431 butylated hydroxytoluene. Then, the mixture was vortexed until colorless
432 (approximately 20 min) and incubated at 30 °C for 10 min. This was followed by
433 centrifugation at 12,000 rpm for 5 min. The acetone phase containing the extracted
434 astaxanthin was filtered through a 0.22-μm membrane for HPLC analysis.
435
436 **PCRTags analysis.**
437 All the synV and synX PCRTags involved in this study are listed in Supplementary
438 Table 2. Amplification of PCRTags was performed using 7.5 μL 2 × Rapid Taq Master
439 Mix (Vazyme Biotech Co., Ltd), 0.4 μL each of forward and reverse primers, 1 μL
440 genomic DNA, and 5.7 μL ddH2O. The reaction procedure was as follows: 95 °C/1 min,
441 35 cycles of 95 °C/20 s, 53 °C/20 s, 72 °C/15 s and a final extension of 72 °C/5 min.
442 Detection of PCRTags was performed by gel electrophoresis.
443
444 **Whole-genome sequencing (WGS) and analysis.**
445 WGS was performed at BGI (Beijing Genomic Institute in Shenzhen, China), and cells
446 were harvested at exponential phase. Libraries were prepared and analyzed using an
447 Illumina HiSeq X-Ten system. The sequencing data were filtered with SOAPnuke

448 (v1.5.2)(Li et al. 2008). and clean reads were stored in FASTQ format for downstream
449 analysis. The read comparison was performed using BWA software with the reference
450 sequence. SVs including insertions, deletions, inversions, intrachromosomal
451 translocations, and interchromosomal translocations were detected using Break Dancer
452 software.
453
454 **Transcriptional analysis.**
455 Yeast cells were harvested from YPD medium at 24 h (exponential phase). Total RNA
456 was extracted using the TRIzol® method following the NEB Next Ultra™ RNA
457 protocol. The concentration of the extracted RNA samples was determined using a
458 NanoDrop system (NanoDrop, Madison, USA), and the integrity of the RNA was
459 examined based on the RNA integrity number (RIN) determined using an Agilent 2100
460 Bioanalyzer (Agilent, Santa Clara, USA). RNA sequencing was carried out by the
461 BGISeq500 platform (BGI-Shenzhen, China). The sequencing data were filtered with
462 SOAPnuke (v1.5.2).(Li et al. 2008)
463 Clean reads were obtained and stored in FASTQ format. The clean reads were mapped
464 to the reference genome using HISAT2 (v2.0.4)(Kim et al. 2015). Bowtie2
465 (v2.2.5)(Langmead and Salzberg 2012) was applied to align the clean reads to the
466 reference coding gene set, and the expression level of each gene was calculated by
467 RSEM (v1.2.12)(Li and Dewey 2011). The heatmap of the gene expression in different
468 samples was drawn by GraphPad Prism (v8.0.1). Essentially, differential expression
469 analysis was performed using DESeq2 (v1.4.5)(Love et al. 2014) with a Q value ≤

470 0.05. To gain insight into the change in phenotype, GO (http://www.geneontology.org/)
471 and KEGG (https://www.kegg.jp/) enrichment analyses of annotated differentially
472 expressed genes were performed by Phyper
473 (https://en.wikipedia.org/wiki/Hypergeometric_distribution) based on the
474 hypergeometric test. Significant terms and pathways were identified as those with
475 Bonferroni-corrected *P*-values below a rigorous threshold (*P*-value ≤ 0.05). Triplicate
476 samples were used for transcriptional analysis. The Saccharomyces Genome Database
477 (SGD)(Cherry et al. 2012) was used to obtain gene information.
478
479 **Hi-C library generation and sequencing.**
480 Hi-C library generation and sequencing were carried out by Frasergen (Wuhan, China),
481 and cells were harvested at exponential phase. Cells were resuspended in 1×PBS to an
482 OD600 of 1.0. Cells were cross-linked in a 3% final concentration of fresh
483 formaldehyde and quenched with glycine (0.15 M final concentration) for 5 min. The
484 cells were resuspended in 1 mL of 1× NEBuffer 2.1 (NEB) and homogenized by
485 grinding to a fine powder in liquid nitrogen. Then, the homogenized yeast material was
486 washed with 25 mL of 1× NEBuffer 2.1 and suspended in 2.5 mL of 1× NEBuffer 2.1.
487 Cells were split into aliquots (V =456 μL) and solubilized in 0.1% SDS for 10 min at
488 65 °C. Cross-linked DNA was digested with 200 U MboI (NEB) per tube at 37 °C
489 overnight. Restriction fragment ends were labeled with biotinylated cytosine
490 nucleotides by biotin-14-dCTP (TriLINK). Blunt-end ligation was carried out at 16 °C
491 overnight in the presence of 100 Weiss units of T4 DNA ligase (Thermo, 10.0 mL final

492 volume per tube).

493 DNA purification was achieved through overnight incubation at 65 °C with 200 μg/mL
494 proteinase K (Thermo). Purified DNA was sheared to a length of ~400 bp. Point ligation
495 junctions were pulled down by Dynabeads® MyOne™ Streptavidin C1 (Thermo
496 Fisher). The Hi-C library for Illumina sequencing was prepared using the NEBNext®
497 Ultra™ II DNA library Prep Kit for Illumina (NEB) according to the manufacturer's
498 instructions. Fragments of between 400 and 600 bp were paired-end sequenced on an
499 Illumina HiSeq X10 platform (San Diego, CA, United States) in 150PEmode. Two
500 replicates were generated for each group of materials.

501

502 **Construction of contact map.**

503 The contact maps were generated using the ICE software package (version
504 1f8815d0cc9e)(Imakaev et al. 2012), and the Hi-C data of YJJ001, YJJ168 and YJJ432
505 cells were iteratively mapped to their own genomes. Dangling ends and other unusable
506 data were filtered out, and the valid pairs were binned into 10 kb nonoverlapping
507 genomic intervals to generate contact maps. The contact maps were normalized using
508 an iterative normalization method to eliminate systematic biases.

509

510 **Cre/loxP induced chromosome translocation and inversion.**

511 Translocations and inversions were detected in YJJ168 and YJJ432 and verified in the
512 wild-type strain BY4741 by introducing two Cre/loxP sites to the corresponding
513 position. LoxP sites were integrated by homologous recombination. Homologous arms

514 upstream and downstream were amplified from the genome of BY4741. Two loxP sites
515 (loxP site 1 and loxP site 2) were integrated along with URA3+ and HIS3+/Hyg- as
516 selection markers. The URA3 promoter was inserted upstream of loxP site 1, and open
517 reading frames of URA3 were inserted downstream of the loxP site, allowing the
518 expression of URA3. Hyg without a promoter was positioned adjacent to downstream
519 loxP site 2 and the HIS3 promoter, and open reading frames of HIS3 were positioned
520 upstream of loxP site 2. Adding 1 μmol L–1 β-estradiol to the cultures to switch on Cre-
521 mediated recombination between the two loxP sites results in translocation and
522 inversion, which subsequently turn on the expression of the Hyg gene and
523 simultaneously shut down URA3 expression. Translocation and inversion strains could
524 be selected on SC-LEU-5-FOA plates and SC-LEU+Hyg.

525 **Data availability.**

526 The data that support the findings of this study are available from the corresponding
527 author on request. Transcriptomes data and Whole-genome sequencing data are
528 available at Sequence Read Archive (SRA) under accession code SUB8866811.

529 **Acknowledgements**

530 This work was funded by Ministry of science and technology the National Key
531 Research and Development Program of China (2021YFC2100800), and the National
532 Natural Science Foundation of China (31800719, 31861143017 and 21621004).

533 **Author contributions**

534 B.J., and J.J. contributed equally to this work. B.J., J.J., and Y.J.Y. designed the
535 experiments. B.J., J.J., and M.Z.H performed the experiments. B.J., J.J., and Y.J.Y.

536 wrote the manuscript and all authors edited the manuscript. This project was supervised
537 by Y.J.Y.

538 **Conflict of Interest**

539 The authors declare no competing financial interests.

540 # Reference

541 Akdemir KC, Le VTT, Chandran S, Li YL, Verhaak RG, Beroukhim R, Campbell PJ, Chin L, Dixon JR,
542 Futreal PA et al. 2020. Disruption of chromatin folding domains by somatic genomic
543 rearrangements in human cancer. *Nature Genetics* **52**: 294-+.

544 Ambati RR, Phang SM, Ravi S, Aswathanarayana RG. 2014. Astaxanthin: Sources, Extraction,
545 Stability, Biological Activities and Its Commercial Applications-A Review. *Mar Drugs* **12**:
546 128-152.

547 Bianco S, Lupianez DG, Chiariello AM, Annunziatella C, Kraft K, Schopflin R, Wittler L, Andrey G,
548 Vingron M, Pombo A et al. 2018. Polymer physics predicts the effects of structural
549 variants on chromatin architecture. *Nature Genetics* **50**: 662-+.

550 Blount BA, Gowers GOF, Ho JCH, Ledesma-Amaro R, Jovicevic D, McKiernan RM, Xie ZX, Li BZ,
551 Yuan YJ, Ellis T. 2018. Rapid host strain improvement by in vivo rearrangement of a
552 synthetic yeast chromosome. *Nature Communications* **9**.

553 Brachmann CB, Davies A, Cost GJ, Caputo E, Li J, Hieter P, Boeke JD. 1998. Designer deletion
554 strains derived from Saccharomyces cerevisiae S288C: a useful set of strains and
555 plasmids for PCR-mediated gene disruption and other applications. *Yeast* **14**: 115-132.

556 Burton JN, Adey A, Patwardhan RP, Qiu RL, Kitzman JO, Shendure J. 2013. Chromosome-scale
557 scaffolding of de novo genome assemblies based on chromatin interactions. *Nat*

558 *Biotechnol* **31**: 1119-+.

559 Chen X, Zhang J. 2016. The Genomic Landscape of Position Effects on Protein Expression Level

560 and Noise in Yeast. *Cell Syst* **2**: 347-354.

561 Cherry JM, Hong EL, Amundsen C, Balakrishnan R, Binkley G, Chan ET, Christie KR, Costanzo MC,

562 Dwight SS, Engel SR et al. 2012. Saccharomyces Genome Database: the genomics

563 resource of budding yeast. *Nucleic Acids Research* **40**: D700-D705.

564 Choudhury S, Baradaran-Mashinchi P, Torres MP. 2018. Negative Feedback Phosphorylation of

565 Ggamma Subunit Ste18 and the Ste5 Scaffold Synergistically Regulates MAPK Activation

566 in Yeast. *Cell Rep* **23**: 1504-1515.

567 Conrad DF, Pinto D, Redon R, Feuk L, Gokcumen O, Zhang YJ, Aerts J, Andrews TD, Barnes C,

568 Campbell P et al. 2010. Origins and functional impact of copy number variation in the

569 human genome. *Nature* **464**: 704-712.

570 Darling AE, Miklos I, Ragan MA. 2008. Dynamics of Genome Rearrangement in Bacterial

571 Populations. *PLoS Genet* **4**: 16.

572 Dekker J, Marti-Renom MA, Mirny LA. 2013. Exploring the three-dimensional organization of

573 genomes: interpreting chromatin interaction data. *Nature Reviews Genetics* **14**: 390-

574 403.

575 Duan Z, Andronescu M, Schutz K, McIlwain S, Kim YJ, Lee C, Shendure J, Fields S, Blau CA, Noble

576 WS. 2010. A three-dimensional model of the yeast genome. *Nature* **465**: 363-367.

577 Dujon B. 2010. Yeast evolutionary genomics. *Nature Reviews Genetics* **11**: 512-524.

578 Dujon B, Sherman D, Fischer G, Durrens P, Casaregola S, Lafontaine I, De Montigny J, Marck C,

579 Neuvéglise C, Talla E et al. 2004. Genome evolution in yeasts. *Nature* **430**: 35-44.

580 Eyupoglu D, Bozkurt S, Haznedaroglu I, Buyukasik Y, Guven D. 2016. The Impact of Variant
581 Philadelphia Chromosome Translocations on the Clinical Course of Chronic Myeloid
582 Leukemia. *Turkish Journal of Hematology* **33**: 60-65.
583 Flagfeldt DB, Siewers V, Huang L, Nielsen J. 2009. Characterization of chromosomal integration
584 sites for heterologous gene expression in Saccharomyces cerevisiae. *Yeast* **26**: 545-551.
585 Fleiss A, O'Donnell S, Fournier T, Lu W, Agier N, Delmas S, Schacherer J, Fischer G. 2019.
586 Reshuffling yeast chromosomes with CRISPR/Cas9. *PLoS Genet* **15**: e1008332.
587 Gao SL, Tong YY, Zhu L, Ge M, Zhang YA, Chen DJ, Jiang Y, Yang S. 2017. Iterative integration of
588 multiple-copy pathway genes in Yarrowia lipolytica for heterologous beta-carotene
589 production. *Metab Eng* **41**: 192-201.
590 Gietz RD, Schiestl RH, Willems AR, Woods RA. 1995. Studies on the transformation of intact yeast
591 cells by the LiAc/SS-DNA/PEG procedure. *Yeast (Chichester, England)* **11**: 355-360.
592 Gowers GOF, Chee SM, Bell D, Suckling L, Kern M, Tew D, McClymont DW, Ellis T. 2020.
593 Improved betulinic acid biosynthesis using synthetic yeast chromosome recombination
594 and semi-automated rapid LC-MS screening. *Nature Communications* **11**.
595 Harewood L, Kishore K, Eldridge MD, Wingett S, Pearson D, Schoenfelder S, Collins VP, Fraser P.
596 2017. Hi-C as a tool for precise detection and characterisation of chromosomal
597 rearrangements and copy number variation in human tumours. *Genome Biology* **18**: 11.
598 Henssen AG, Koche R, Zhuang J, Jiang E, Reed C, Eisenberg A, Still E, MacArthur IC, Rodriguez-
599 Fos E, Gonzalez S et al. 2017. PGBD5 promotes site-specific oncogenic mutations in
600 human tumors. *Nature Genetics* **49**: 1005-+.
601 Igielska-Kalwat J, Goscianska J, Nowak I. 2015. Carotenoids as natural antioxidants. *Postepy*

602 *higieny i medycyny doswiadczalnej (Online)* **69**: 418-428.

603 Imakaev M, Fudenberg G, McCord RP, Naumova N, Goloborodko A, Lajoie BR, Dekker J, Mirny
604 LA. 2012. Iterative correction of Hi-C data reveals hallmarks of chromosome
605 organization. *Nat Methods* **9**: 999-+.

606 Jia B, Wu Y, Li B-Z, Mitchell LA, Liu H, Pan S, Wang J, Zhang H-R, Jia N, Li B et al. 2018. Precise
607 control of SCRaMbLE in synthetic haploid and diploid yeast. *Nature Communications* **9**.

608 Jin J, Wang Y, Yao M, Gu X, Li B, Liu H, Ding M, Xiao W, Yuan Y. 2018. Astaxanthin
609 overproduction in yeast by strain engineering and new gene target uncovering.
610 *Biotechnology for Biofuels* **11**.

611 Kidd JM, Cooper GM, Donahue WF, Hayden HS, Sampas N, Graves T, Hansen N, Teague B, Alkan
612 C, Antonacci F et al. 2008. Mapping and sequencing of structural variation from eight
613 human genomes. *Nature* **453**: 56-64.

614 Kim D, Landmead B, Salzberg SL. 2015. HISAT: a fast spliced aligner with low memory
615 requirements. *Nat Methods* **12**: 357-U121.

616 Langmead B, Salzberg SL. 2012. Fast gapped-read alignment with Bowtie 2. *Nat Methods* **9**:
617 357-U354.

618 Li B, Dewey CN. 2011. RSEM: accurate transcript quantification from RNA-Seq data with or
619 without a reference genome. *BMC Bioinformatics* **12**: 16.

620 Li RQ, Li YR, Kristiansen K, Wang J. 2008. SOAP: short oligonucleotide alignment program.
621 *Bioinformatics* **24**: 713-714.

622 Li Y, Wu Y, Ma L, Guo Z, Xiao W, Yuan Y. 2019. Loss of heterozygosity by SCRaMbLEing. *Science*
623 *China Life Sciences* **62**: 381-393.

624 Lieberman-Aiden E, van Berkum NL, Williams L, Imakaev M, Ragoczy T, Telling A, Amit I, Lajoie
625 BR, Sabo PJ, Dorschner MO et al. 2009. Comprehensive Mapping of Long-Range
626 Interactions Reveals Folding Principles of the Human Genome. *Science* **326**: 289-293.
627 Liu W, Luo Z, Wang Y, Pham NT, Tuck L, Pérez-Pi I, Liu L, Shen Y, French C, Auer M et al. 2018.
628 Rapid pathway prototyping and engineering using in vitro and in vivo synthetic genome
629 SCRaMbLE-in methods. *Nature Communications* **9**.
630 Love MI, Huber W, Anders S. 2014. Moderated estimation of fold change and dispersion for
631 RNA-seq data with DESeq2. *Genome Biology* **15**: 38.
632 Luo Z, Wang L, Wang Y, Zhang W, Guo Y, Shen Y, Jiang L, Wu Q, Zhang C, Cai Y et al. 2018.
633 Identifying and characterizing SCRaMbLEd synthetic yeast using ReSCuES. *Nature*
634 *Communications* **9**.
635 Ma L, Li Y, Chen X, Ding M, Wu Y, Yuan Y-J. 2019. SCRaMbLE generates evolved yeasts with
636 increased alkali tolerance. *Microbial Cell Factories* **18**.
637 Natesuntorn W, Iwami K, Matsubara Y, Sasano Y, Sugiyama M, Kaneko Y, Harashima S. 2015.
638 Genome-wide construction of a series of designed segmental aneuploids in
639 Saccharomyces cerevisiae. *Scientific Reports* **5**.
640 Nishikawa M, Ichiyama T, Hayashi T, Furukawa S. 1997. Mobius-like syndrome associated with a
641 1;2 chromosome translocation. *Clinical genetics* **51**: 122-123.
642 Pang AW, MacDonald JR, Pinto D, Wei J, Rafiq MA, Conrad DF, Park H, Hurles ME, Lee C, Venter
643 JC et al. 2010. Towards a comprehensive structural variation map of an individual human
644 genome. *Genome Biology* **11**.
645 Peter J, De Chiara M, Friedrich A, Yue JX, Pflieger D, Bergstrom A, Sigwalt A, Barre B, Freel K,

646 Llored A et al. 2018. Genome evolution across 1,011 Saccharomyces cerevisiae isolates.
647 *Nature* **556**: 339-+.
648 Pevzner P, Tesler G. 2003. Genome Rearrangements in mammalian evolution: Lessons from
649 human and mouse genomes. *Genome Research* **13**: 37-45.
650 Poddar A, Roy N, Sinha P. 1999. MCM21and MCM22, two novel genes of the yeast
651 Saccharomyces cerevisiae are required for chromosome transmission. *Molecular*
652 *Microbiology* **31**: 349–360.
653 Puddu F, Herzog M, Selivanova A, Wang SY, Zhu J, Klein-Lavi S, Gordon M, Meirman R, Millan-
654 Zambrano G, Ayestaran I et al. 2019. Genome architecture and stability in the
655 Saccharomyces cerevisiae knockout collection. *Nature* **573**: 416-+.
656 Rao SSP, Huntley MH, Durand NC, Stamenova EK, Bochkov ID, Robinson JT, Sanborn AL, Machol
657 I, Omer AD, Lander ES et al. 2014. A 3D Map of the Human Genome at Kilobase
658 Resolution Reveals Principles of Chromatin Looping. *Cell* **159**: 1665-1680.
659 Redon R, Ishikawa S, Fitch KR, Feuk L, Perry GH, Andrews TD, Fiegler H, Shapero MH, Carson AR,
660 Chen WW et al. 2006. Global variation in copy number in the human genome. *Nature*
661 **444**: 444-454.
662 Rickman DS, Soong TD, Moss B, Mosquera JM, Dlabal J, Terry S, MacDonald TY, Tripodi J,
663 Bunting K, Najfeld V et al. 2012. Oncogene-mediated alterations in chromatin
664 conformation. *Proceedings of the National Academy of Sciences of the United States of*
665 *America* **109**: 9083-9088.
666 Saliba AE, Westermann AJ, Gorski SA, Vogel J. 2014. Single-cell RNA-seq: advances and future
667 challenges. *Nucleic Acids Res* **42**: 8845-8860.

668 Selmecki AM, Maruvka YE, Richmond PA, Guillet M, Shoresh N, Sorenson AL, De S, Kishony R,
669 Michor F, Dowell R et al. 2015. Polyploidy can drive rapid adaptation in yeast. *Nature*
670 **519**: 349-352.
671 Shen MJ, Wu Y, Yang K, Li Y, Xu H, Zhang H, Li B-Z, Li X, Xiao W-H, Zhou X et al. 2018.
672 Heterozygous diploid and interspecies SCRaMbLEing. *Nature Communications* **9**.
673 Si T, Xiao H, Zhao H. 2015. Rapid prototyping of microbial cell factories via genome-scale
674 engineering. *Biotechnol Adv* **33**: 1420-1432.
675 Sotoudeh A, Rostami P, Nakhaeimoghadam M, Mohsenipour R, Rezaei N. 2017. Pericentric
676 Inversion of Chromosome 9 in an Infant With Ambiguous Genitalia. *Acta medica Iranica*
677 **55**: 655-657.
678 Wang J, Jia B, Xie ZX, Li YX, Yuan YJ. 2018. Improving prodeoxyviolacein production via multiplex
679 SCRaMbLE iterative cycles. *Front Chem Sci Eng* **12**: 806-814.
680 Wang R, Gu X, Yao M, Pan C, Liu H, Xiao W, Wang Y, Yuan Y. 2017. Engineering of β-carotene
681 hydroxylase and ketolase for astaxanthin overproduction in Saccharomyces cerevisiae.
682 *Frontiers of Chemical Science and Engineering* **11**: 89-99.
683 Wu T, Ye LJ, Zhao DD, Li SW, Li QY, Zhang BL, Bi CH, Zhang XL. 2017a. Membrane engineering -
684 A novel strategy to enhance the production and accumulation of beta-carotene in
685 Escherichia coli. *Metab Eng* **43**: 85-91.
686 Wu X-L, Li B-Z, Zhang W-Z, Song K, Qi H, Dai J-b, Yuan Y-J. 2017b. Genome-wide landscape of
687 position effects on heterogeneous gene expression in Saccharomyces cerevisiae.
688 *Biotechnology for Biofuels* **10**.
689 Wu Y, Li BZ, Zhao M, Mitchell LA, Xie ZX, Lin QH, Wang X, Xiao WH, Wang Y, Zhou X et al.

690 2017c. Bug mapping and fitness testing of chemically synthesized chromosome X.
691 *Science* **355**: 7.
692 Wu Y, Zhu R-Y, Mitchell LA, Ma L, Liu R, Zhao M, Jia B, Xu H, Li Y-X, Yang Z-M et al. 2018. In
693 vitro DNA SCRaMbLE. *Nature Communications* **9**.
694 Xie ZX, Li BZ, Mitchell LA, Wu Y, Qi X, Jin Z, Jia B, Wang X, Zeng BX, Liu HM et al. 2017. "Perfect"
695 designer chromosome V and behavior of a ring derivative. *Science* **355**: 8.
696 Yue JX, Li J, Aigrain L, Hallin J, Persson K, Oliver K, Bergstrom A, Coupland P, Warringer J,
697 Lagomarsino MC et al. 2017. Contrasting evolutionary genome dynamics between
698 domesticated and wild yeasts. *Nature Genetics* **49**: 913-+.
699 Zhou PP, Ye LD, Xie WP, Lv XM, Yu HW. 2015. Highly efficient biosynthesis of astaxanthin in
700 Saccharomyces cerevisiae by integration and tuning of algal crtZ and bkt. *Appl*
701 *Microbiol Biotechnol* **99**: 8419-8428.
702
703

704 **Table 1 *S. cerevisiae* strains used in this study**

Strains	Description	Sources
BY4741	*MATa, HIS3Δ1, LEU2Δ0, MET15Δ0, URA3Δ0*	(Brachmann et al. 1998)
SYNVX	*MATa, HIS3Δ1, LEU2Δ0, MET15Δ0, URA3Δ0*	This study
YJJ001	yXZX573, CAN1:: astaxanthin pathway with Leu2 marker	This study
YJJ002	Introducing plasmid pGAL1-Cre-EBD-GFP-tCYC1 into strain YJJ001	This study
YJJ168	SCRaMbLEd strain from the YJJ002	This study
YJJ432	SCRaMbLEd strain from the YJJ168	This study
YJJ468	Astaxanthin producing strain, BY4741	This study
YJJ473	YJJ468 with inversion (YJL052C-A-YJR071C) strain	This study
YJJ474	YJJ468 with translocation (YJR130C and YER164W) strain	This study
YJJ522	YJJ001 with YJL053Woverexpression	This study
YJJ523	YJJ001 with YJL052C-A overexpression	This study
YJJ524	YJJ001 with YJL052W deletion	This study
YJJ525	YJJ001 with YJL049W overexpression	This study
YJJ526	YJJ001 with YJL046W overexpression	This study
YJJ527	YJJ001 with YJL045W overexpression	This study
YJJ528	YJJ001 with YJR067C overexpression	This study
YJJ529	YJJ001 with YJR068W overexpression	This study
YJJ530	YJJ001 with YJR070C overexpression	This study
YJJ531	YJJ001 with YJR071W overexpression	This study
YJJ532	YJJ001 with YJR072C overexpression	This study
YJJ533	YJJ001 with YJR076C overexpression	This study
YJJ534	YJJ001 with YJR079W overexpression	This study
YJJ535	YJJ001 with YJR080C overexpression	This study
YJJ536	YJJ001 with YJR082C overexpression	This study
YJJ537	YJJ001 with YJR085C overexpression	This study
YJJ538	YJJ001 with YJR086W overexpression	This study
YJJ539	YJJ001 with YJR087W overexpression	This study
YJJ540	YJJ001 with YJR088C overexpression	This study
YJJ541	YJJ001 with YER156C overexpression	This study
YJJ542	YJJ001 with YER158C deletion	This study
YJJ543	YJJ001 with YER163C overexpression	This study
YJJ544	YJJ001 with YER168C overexpression	This study
YJJ545	YJJ001 with YER170W overexpression	This study
YJJ546	YJJ001 with YJR122W overexpression	This study
YJJ547	YJJ001 with YJR123W overexpression	This study
YJJ548	YJJ001 with YJR127 deletion	This study
YJJ549	YJJ001 with YJR125C overexpression	This study
YJJ551	YJJ001 with YJR133W overexpression	This study
YJJ552	YJJ001 with YJR135C overexpression	This study
YJJ553	YJJ001 with YJR135W-A overexpression	This study
YJJ554	YJJ001 with YJR136C overexpression	This study

705

706 **Table 2** Known gene functions for beneficial over-expression

Gene	Description
YJR086W(STE18)	G protein gamma subunit; forms a dimer with Ste4p to activate the mating signaling pathway, forms a heterotrimer with Gpa1p and Ste4p to dampen signaling; C-terminus is palmitoylated and farnesylated, which are required for normal signaling
YJR123W(RPS5)	Protein component of the small (40S) ribosomal subunit; least basic of non-acidic ribosomal proteins; phosphorylated in vivo; essential for viability; homologous to mammalian ribosomal protein S5 and bacterial S7
YJR135C(MCM22)	Outer kinetochore protein and component of the Ctf3 subcomplex; binds to centromeric DNA in a Ctf19p-dependent manner; involved in chromosome segregation and minichromosome maintenance; orthologous to human centromere constitutive-associated network (CCAN) subunit CENP-K and fission yeast sim4

707

708

709

710

711

712

713

714 **Fig. 1 SCRaMbLE with two synthetic chromosomes generating complex SVs. a,**
715 **Schematic representation of structural variations in YJJ001, YJJ168 and YJJ432.**
716 **Synthetic chromosome V and synthetic chromosome X are abbreviated as synV**
717 **and synX, respectively. b, Normalized contact maps (bin size, 2 kb) of synthetic**
718 **chromosomes in three different strains: YJJ117, YJJ168 and YJJ432. All Hi-C**
719 **reads are mapped against the reference genome of the parental strain YJJ001. c,**
720 **Three-dimensional model of the YJJ001, YJJ168 and YJJ432 genomes. Synthetic**
721 **chromosomes and wild chromosomes are indicated with graduated color and gray,**
722 **respectively. The SV area are indicated with the dashed oval. d, The astaxanthin**
723 **yield of control strain YJJ001 and SCRaMbLEd strains YJJ168 and YJJ432.**
724

725

726 **Fig. 2 Quantified interactions of loxP breakpoint-flanking regions. a, Triangle heat**
727 **maps representing the contact frequencies among 20 bin regions (length 20 kb)**
728 **upstream and downstream of two recombination sites (YJL052C-A and YJR071C)**
729 **in YJJ168, labeled A, B, C, and D. Dots show fold changes in expression in the A,**
730 **B, C, and D regions. b, Triangle heat maps representing the contact frequencies**
731 **among 20 bin regions (length 20 kb) upstream and downstream of the two**
732 **recombination sites (YER164W and YJR130C) in YJJ432, labeled E, F, G, and H.**
733 **Dots show fold changes in expression in the E, F, G, H regions.**
734

735

736 **Fig. 3 a, The astaxanthin yield of control strain YJJ001 and genes overexpression**

737 **and deletion around pericentric inversion strain breakpoint-flanking regions and**

738 **genes overexpression and deletion around trans-chromosomic translocation strain**

739 **breakpoint-flanking regions. (Student's t-test; *P < 0.05). b, Enrichment analysis**

740 **of transcriptomics of YJJ168 and YJJ432 were used to identify differentially**

741 **transcribed genes with known functions involved in KEGG pathways.**

742

743

744 **Fig. 4 Rational translocation and inversion of chromosomes. a, The process of**
745 **inversion and translocation was validated in wild-type strains. Wild-type**
746 **chromosome V and wild-type chromosome X are abbreviated as wt V and wt X,**
747 **respectively. Validation strains exhibited inversion and translocation events**
748 **between two LoxP sites. These events were identified by aligning all raw reads. b,**
749 **Verification of inversion and translocation by junction PCR. c, The astaxanthin**
750 **yield of the wild-type control strain YJJ468, inversion strain YJJ473 and**
751 **translocation strain YJJ474. Serial dilution assay of YJJ468, YJJ473, YJJ474.**
752

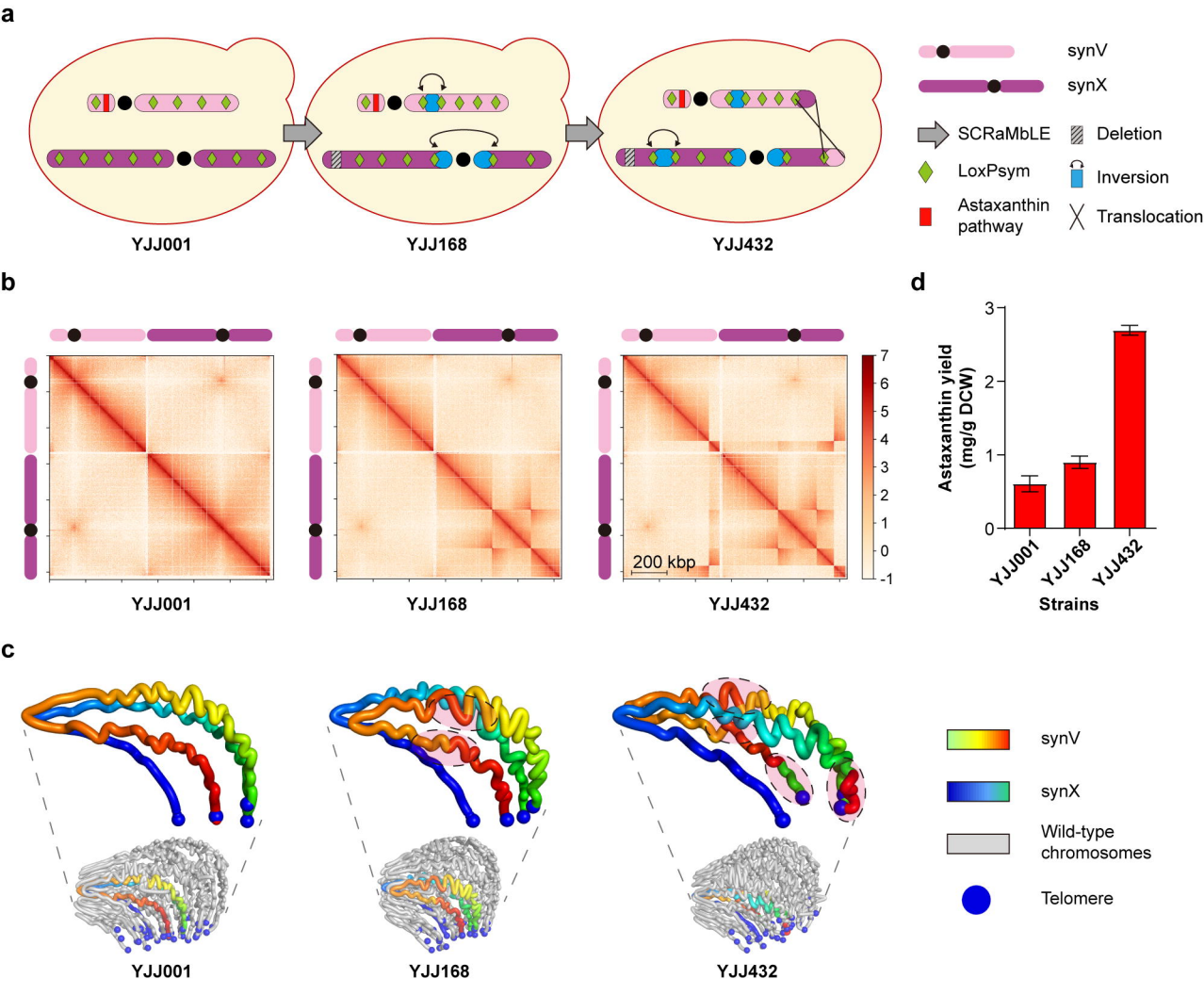
a
YJJ001
YJJ168
YJJ432
synV
synX
SCRaMbLE
Deletion
LoxPsym
Inversion
Astaxanthin pathway
Translocation
b
YJJ001
YJJ168
YJJ432
200 kbp
7
6
5
4
3
2
1
0
-1
d
Astaxanthin yield (mg/g DCW)
3
2
1
0
YJJ001
YJJ168
YJJ432
Strains
c
YJJ001
YJJ168
YJJ432
synV
synX
Wild-type chromosomes
Telomere

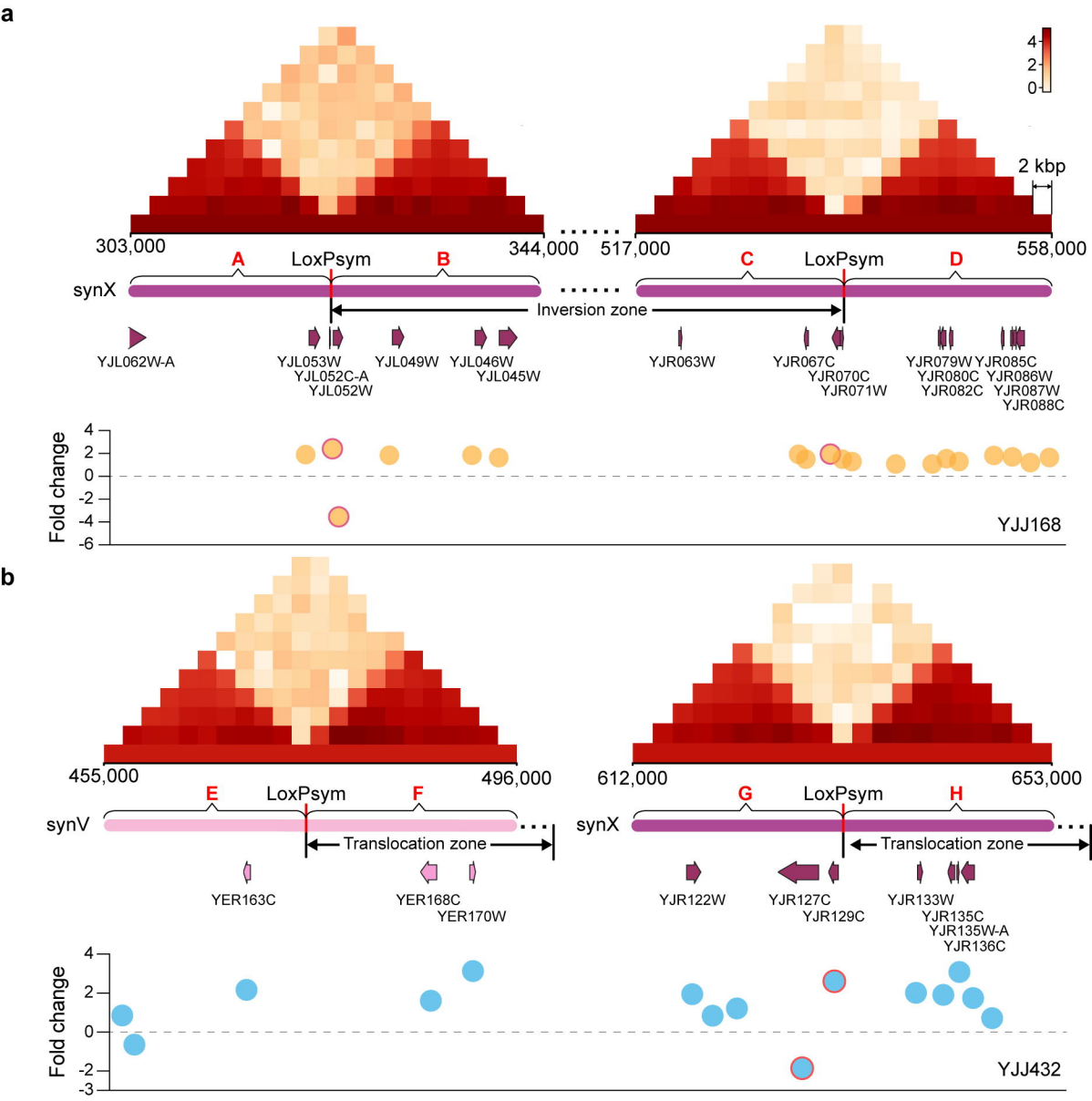
a
4
2
0
2 kbp
303,000
344,000
517,000
558,000
A
LoxPsym
B
C
LoxPsym
D
synX
Inversion zone
YJL062W-A
YJL053W
YJL052C-A
YJL052W
YJL049W
YJL046W
YJL045W
YJR063W
YJR067C
YJR070C
YJR071W
YJR079W
YJR080C
YJR082C
YJR085C
YJR086W
YJR087W
YJR088C
Fold change
4
2
0
-2
-4
-6
YJJ168
b
455,000
496,000
612,000
653,000
E
LoxPsym
F
G
LoxPsym
H
synV
Translocation zone
synX
Translocation zone
YER163C
YER168C
YER170W
YJR122W
YJR127C
YJR129C
YJR133W
YJR135C
YJR135W-A
YJR136C
Fold change
4
2
0
-2
-3
YJJ432

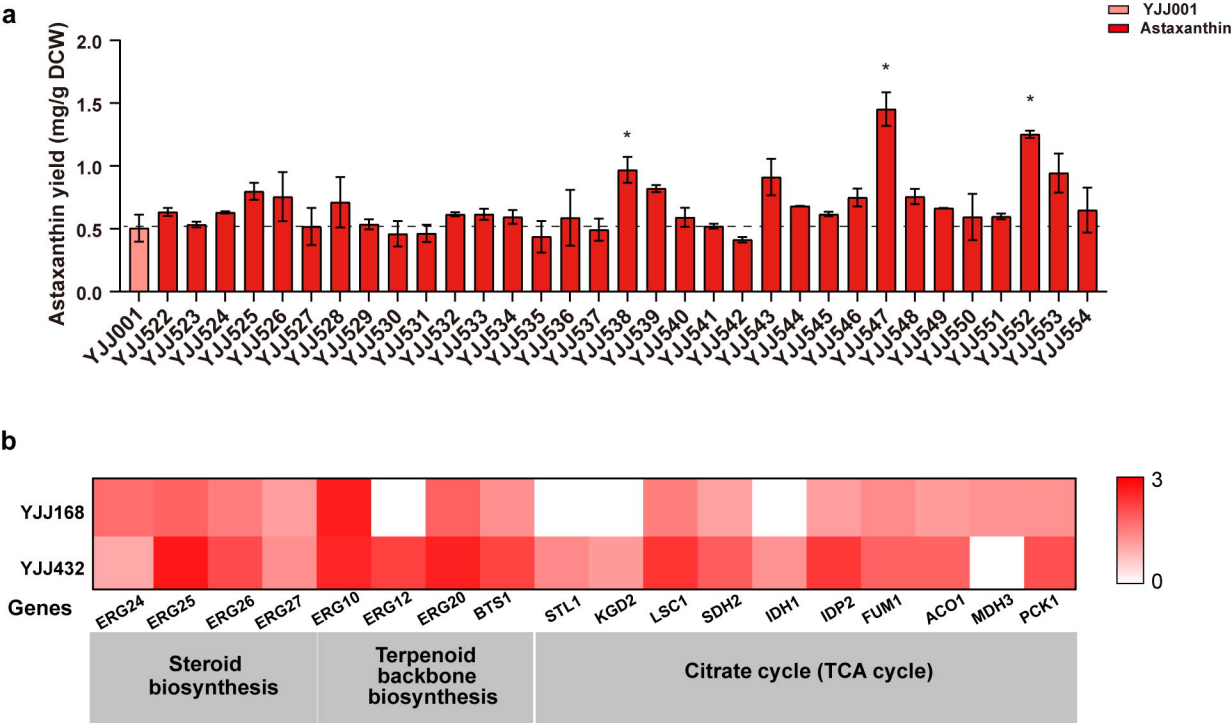
a
YJJ001
Astaxanthin
Astaxanthin yield (mg/g DCW)
2.0
1.5
1.0
0.5
0.0
*
*
*
YJJ001
YJJ522
YJJ523
YJJ524
YJJ525
YJJ526
YJJ527
YJJ528
YJJ529
YJJ530
YJJ531
YJJ532
YJJ533
YJJ534
YJJ535
YJJ536
YJJ537
YJJ538
YJJ539
YJJ540
YJJ541
YJJ542
YJJ543
YJJ544
YJJ545
YJJ546
YJJ547
YJJ548
YJJ549
YJJ550
YJJ551
YJJ552
YJJ553
YJJ554
b
YJJ168
YJJ432
Genes
ERG24
ERG25
ERG26
ERG27
ERG10
ERG12
ERG20
BTS1
STL1
KGD2
LSC1
SDH2
IDH1
IDP2
FUM1
ACO1
MDH3
PCK1
3
0
Steroid biosynthesis
Terpenoid backbone biosynthesis
Citrate cycle (TCA cycle)

a

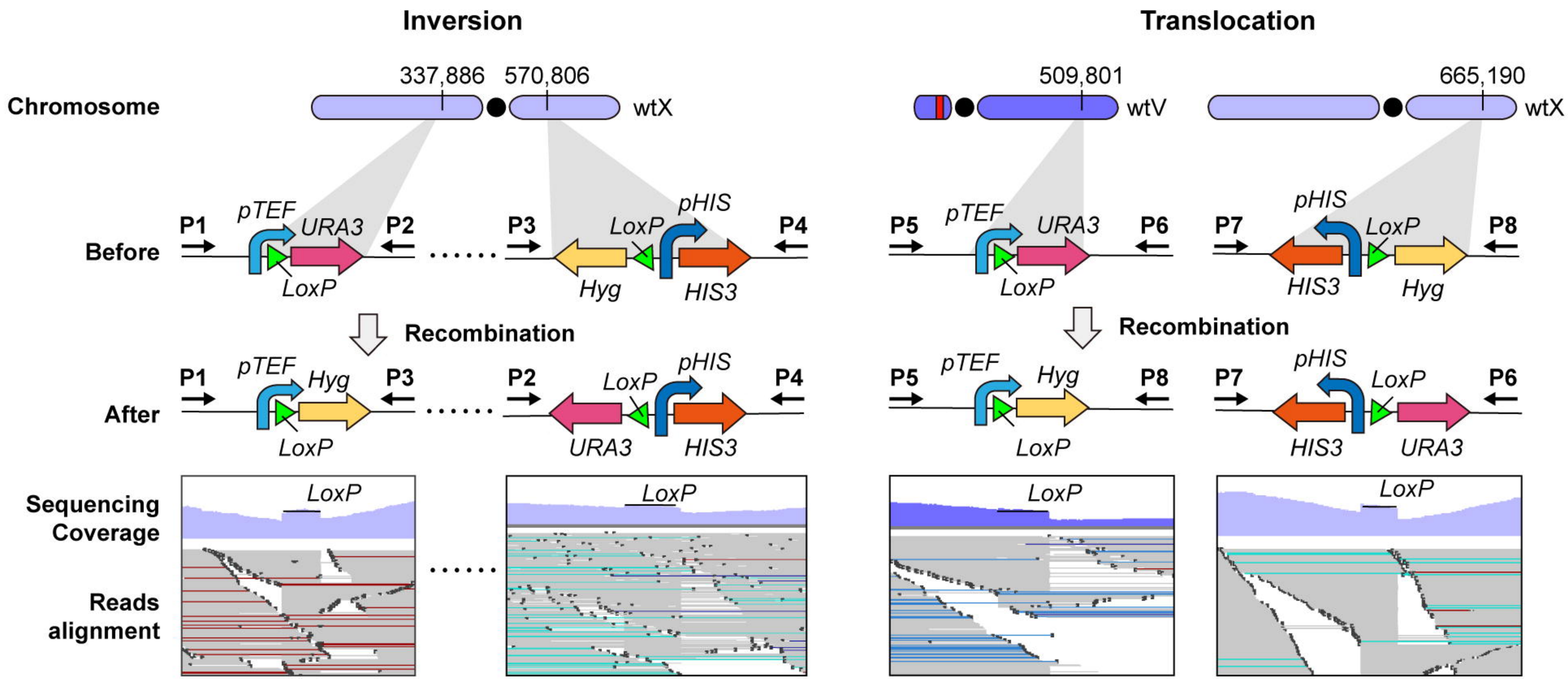
Inversion
Translocation
Chromosome
337,886
570,806
wtX
509,801
wtV
665,190
wtX
Before
P1
pTEF
URA3
P2
P3
LoxP
pHIS
P4
LoxP
Hyg
HIS3
P5
pTEF
URA3
P6
P7
pHIS
LoxP
P8
LoxP
HIS3
Hyg
Recombination
After
P1
pTEF
Hyg
P3
P2
LoxP
pHIS
P4
LoxP
URA3
HIS3
P5
pTEF
Hyg
P8
P7
pHIS
LoxP
P6
LoxP
HIS3
URA3
Sequencing Coverage
Reads alignment
LoxP
LoxP
LoxP
LoxP

b

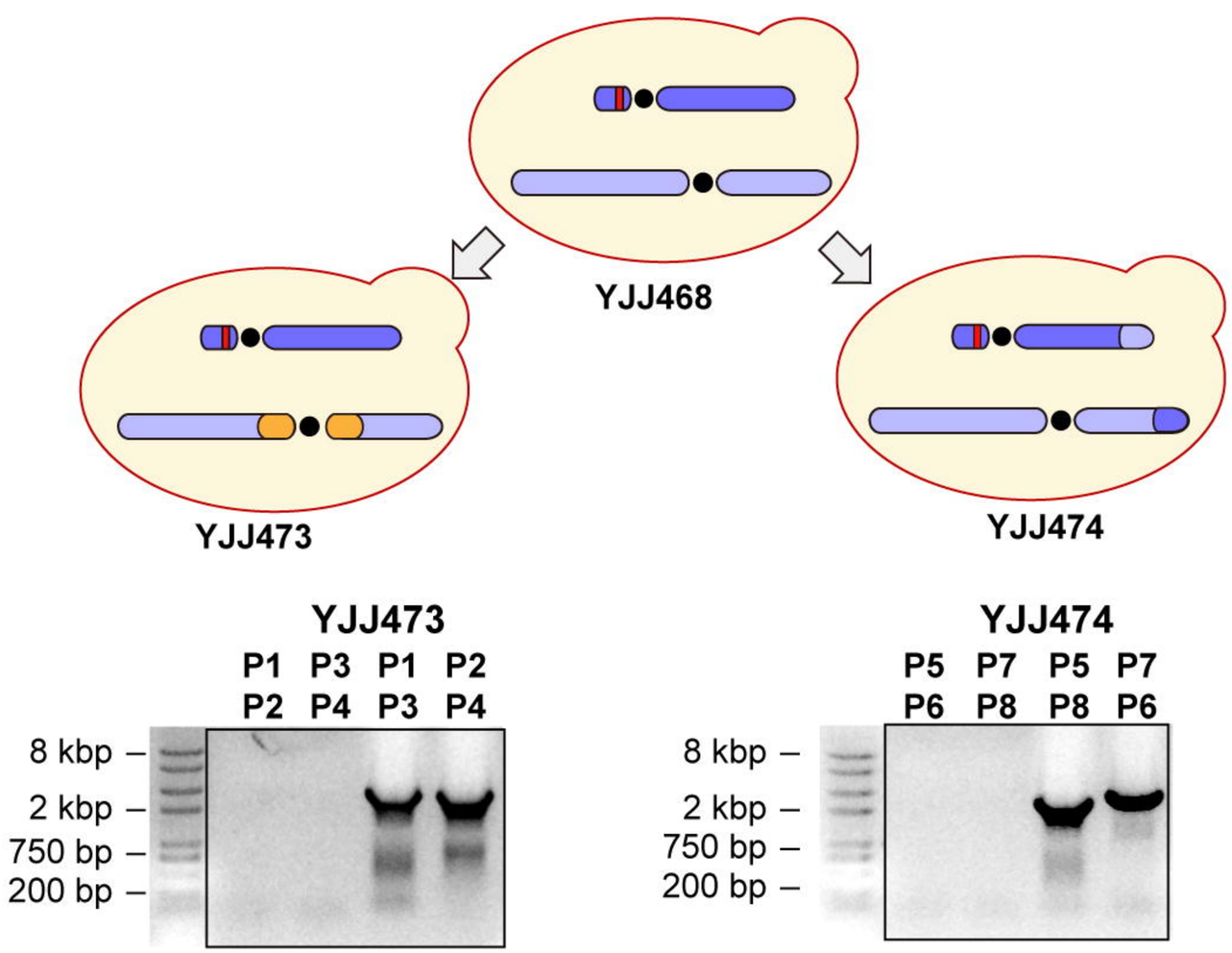
YJJ468
YJJ473
YJJ474
YJJ473
P1 P3 P1 P2
P2 P4 P3 P4
8 kbp
2 kbp
750 bp
200 bp
YJJ474
P5 P7 P5 P7
P6 P8 P8 P6
8 kbp
2 kbp
750 bp
200 bp

c

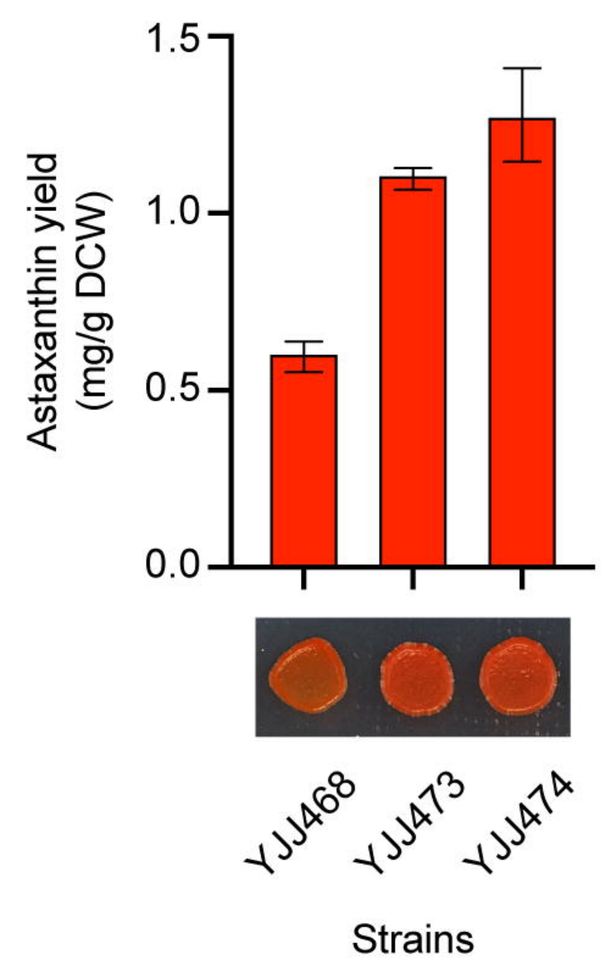
Astaxanthin yield (mg/g DCW)
1.5
1.0
0.5
0.0
YJJ468
YJJ473
YJJ474
Strains